Importance of the 4p states of As and the interlayer cation states in LaFe$_2$As$_2$ and CaFe$_2$As$_2$

Ming-Cui Ding [1,*] Bing-Ying Pan,[1] Gang Zhao,[1] and Yu-Zhong Zhang[2,†]

[1]*School of Physics and Optoelectronic Engineering, Ludong University, Yantai 264025, People's Republic of China*
[2]*Shanghai Key Laboratory of Special Artificial Microstructure Materials and Technology, School of Physics Science and Engineering, Tongji University, Shanghai 200092, People's Republic of China*

The electronic structures of the UT and CT phases of both LaFe$_2$As$_2$ and the counterpart CaFe$_2$As$_2$ are studied by density functional theory and tight-binding models. We find the 4p states of As contribute substantially to the relative instability between (π, π, π) and $(0, 0, \pi)$ of Pauli susceptibility χ_0, which may result in fluctuations mediating the pairing between electrons. This means that considering only the 3d states of Fe is not enough to capture the superconducting properties of iron-based superconductors. This finding is supported by the even higher relative instability at (π, π, π) of interorbital Pauli susceptibility between the 3d orbital of Fe and 4p orbital of As compared with the total intraorbital and interorbital Pauli susceptibility from the 3d orbital of Fe, indicating that the 4p states of As affect χ_0 considerably. Moreover, while the 3d states of Ca are found to contribute positively to the relative instability at (π, π, π), the 5d states of La contribute negatively to the relative instability at (π, π, π), illustrating the the 3d states of Ca and 5d states of La play contrary contributions to superconductivity. Our results provide qualitative criteria for the superconducting properties of LaFe$_2$As$_2$ and CaFe$_2$As$_2$, and they reveal that both the 4p states of As and interlayer cation states should not be neglected in further studies on superconductivity of iron-based superconductors.

I. INTRODUCTION

A distinguishing feature of the iron-based superconductor is that electrons occupy multiple orbitals [1–3]. It is generally believed that 3d states of Fe which locate close to the Fermi level control the magnetic and superconducting properties of iron-based superconductors [4,5]. In this general context, different models have been constructed to capture the electronic pairing mechanism of iron-based superconductors, such as the two-orbital model [6,7], three-orbital model [8,9], and five-orbital model [10,11]. The 4p orbital of As or Se were also included in the so-called d-p model in some iron-based superconductors due to the strong hybridization between the d and p states [12]. Later it is found iron germanides have a general tendency toward ferromagnetism due to the intercalating species [13]. However, an appealing question still subsistent is what role of 4p states of As and the interlayer cation states play on the superconducting properties of iron-based superconductors.

Recently a new 122-type iron-based superconductor LaFe$_2$As$_2$ attracts much attention to study the effect of doping and structural distortion on superconductivity [14–19]. Due to different crystal growth and annealing conditions, LaFe$_2$As$_2$ can be grown in the collapsed tetragonal (CT) phase and uncollapsed tetragonal (UT) phase. The UT phase of LaFe$_2$As$_2$ show superconductivity at 12.1K, while neither superconductivity nor long-range magnetic order was found

in the CT phase of LaFe$_2$As$_2$ [14]. Contrasting properties exist in the counterpart CaFe$_2$As$_2$, the UT phase of CaFe$_2$As$_2$ at atmospheric pressure shows stripe-type antiferromagnetic order at low temperature [20,21]. Superconductivity emerges with Tc up to 12 K by nonhydrostatic pressure for CaFe$_2$As$_2$ [22]. Later it is found the uncollapsed stabilized tetragonal phase(UT′) under uniaxial pressure is responsible for superconductivity [23]. The CT phases of both LaFe$_2$As$_2$ and CaFe$_2$As$_2$ are nonmagnetic and nonsuperconducting [14,21,24]. Analogous structures with diverse magnetic and superconducting properties in these iron-based materials deserve a comparative DFT calculation.

Compared with CaFe$_2$As$_2$, there is one more valence 5d electron of La in LaFe$_2$As$_2$. The effects of the 5d states of La on the electronic structure and the doping level of the 5d electron have been studied by DFT and DFT + DMFT [15,16]. So far, however, a direct relation between superconductivity and the intercalating cations Ca or La in these 122 type iron-based superconductors is still lacking.

In this paper, we derive important qualitative relations between the orbital resolved Pauli susceptibility χ_0 and magnetic or superconducting properties of a series 122 type iron-based superconductors. We apply density functional calculations to both the UT and CT phases of LaFe$_2$As$_2$ and CaFe$_2$As$_2$. By constructing tight-binding models including the 3d orbital of Fe, 4p orbital of As, and 3d orbital of Ca or 5d orbital of La from electronic structures obtained by DFT calculations, we identify the usually overlooked 4p states of As contributing substantially to the relative instability between (π, π, π) and $(0, 0, \pi)$ of Pauli susceptibility χ_0 in both the UT phase of LaFe$_2$As$_2$ and the CT phase of CaFe$_2$As$_2$. Moreover, the 3d
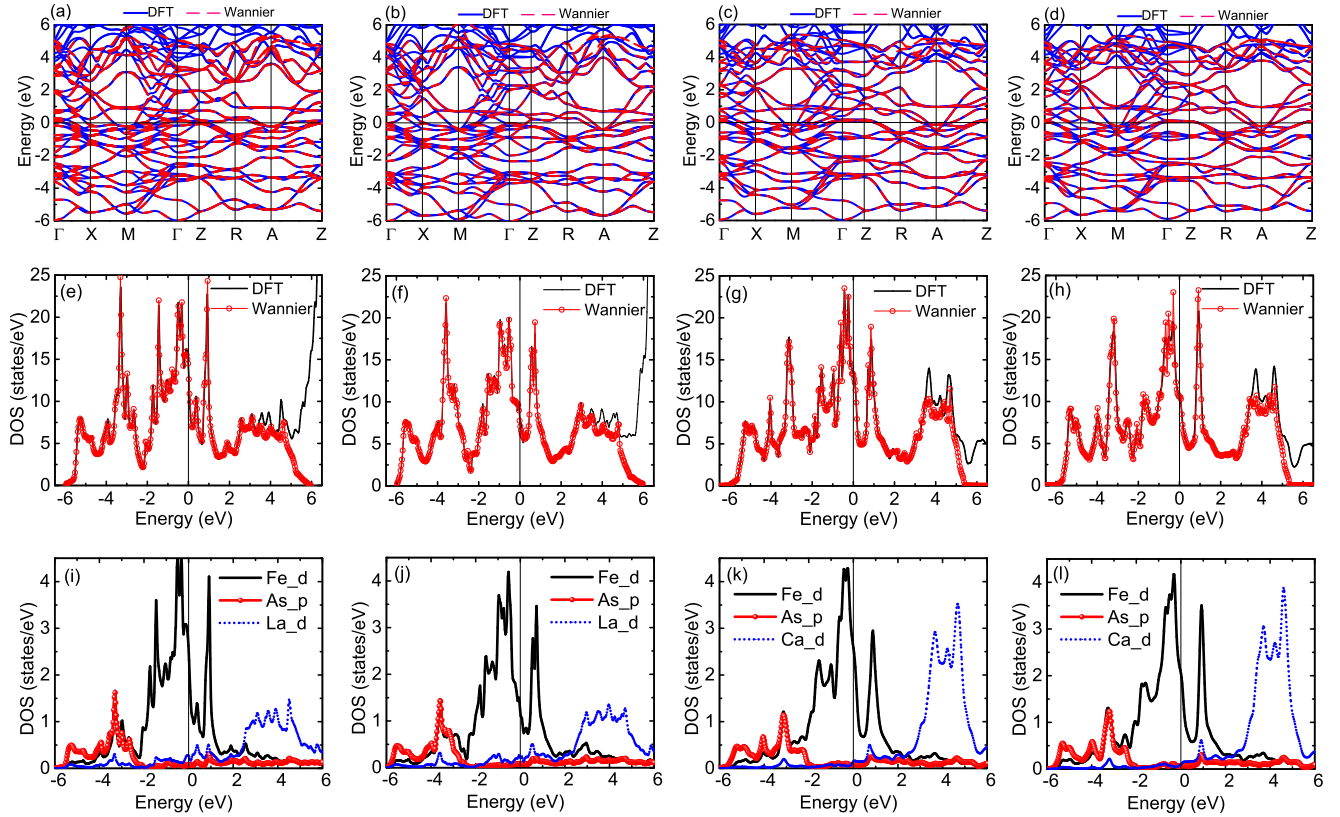
FIG. 1. Comparison of band structure calculated from density functional theory and effective tight-binding model for the UT phase of LaFe$_2$As$_2$ (a), the CT phase of LaFe$_2$As$_2$ (b), the UT phase of CaFe$_2$As$_2$ (c), the UT$'$ phase of CaFe$_2$As$_2$ (d), and the reciprocal points in the bulk Brillouin zone are Γ $(0, 0, 0)$, X $(0, \pi, 0)$, M $(\pi, \pi, 0)$, Z $(0, 0, \pi)$, R $(0, \pi, \pi)$, and A (π, π, π). Comparison of DOS calculated from density functional theory and effective tight-binding model for the UT phase of LaFe$_2$As$_2$ (e), the CT phase of LaFe$_2$As$_2$ (f), the UT phase of CaFe$_2$As$_2$ (g), and the UT$'$ phase of CaFe$_2$As$_2$ (h). Partial density of states for the UT phase of LaFe$_2$As$_2$ (i), the CT phase of LaFe$_2$As$_2$ (j), the UT phase of CaFe$_2$As$_2$ (k), and the UT$'$ phase of CaFe$_2$As$_2$ (l).

orbital of Ca and the 5d orbital of La usually been classified as charge reservoirs are found to affect oppositely to the instability at (π, π, π). While the 3d states of Ca help to enhance the relative instability at (π, π, π) of χ_0, the 5d states of La weaken the relative instability at (π, π, π) of χ_0, which may suppress Tc of superconductivity in LaFe$_2$As$_2$. Furthermore, we find the 5d electron of La does not dope to the 3d orbital of Fe, instead, electrons are re-distributed among the partial orbitals in the different phases LaFe$_2$As$_2$ and CaFe$_2$As$_2$, which results in different orbital resolved particle-hole excitations in these iron-based materials.

II. DETAILS OF OUR CALCULATIONS

DFT calculations were performed using the full potential linearized augmented plane-wave method as implemented in the WIEN2K code [25]. The generalized gradient approximation of Perdew-Burke-Ernzerhhor for exchange-correlation potentials [26] was adopted. To determine the orbital resolved particle-hole excitation properties, tight-binding models from maximally localized Wannier functions [27,28] including the 3d orbital of Fe, the 4p orbital of As, and the 3d orbital of Ca or the 5d orbital of La were constructed. We can see both the band structure and the density states of the effective tight-binding model are well consistent with density func-

tional theory as shown in Figs. 1(a)–1(h), The experimental lattice structures [14] were used for UT and CT phases of LaFe$_2$As$_2$, The experimental lattice structures of CaFe$_2$As$_2$ [20] were used for the CT phase with $a = 3.9724$ Å, $c = 10.683$ Å, the UT$'$ phase(uncollapsed tetragonal phase at a pressure $p = 0.63$ GPa) with $a = 3.8944$ Å, $c = 11.530$ Å and the UT phase (uncollapsed tetragonal phase at a pressure $p = 0$ GPa) with $a = 3.8915$ Å, $c = 11.690$ Å. we found the conclusion did not alter when the other experiment lattice structure of CaFe$_2$As$_2$ was used [29].The coordinate system we adopted points along the iron diagonal, which is the same as experimental works, and the conclusions of our paper are independent on the coordinates we choose.

The Pauli susceptibility [30] is defined as

$$\chi_0^{pr;st}(k, \omega) = -\frac{1}{N} \sum_{k,\mu\nu} \frac{a_\mu^s(k)a_\mu^{p*}(k)a_\nu^r(k+q)a_\nu^{t*}(k+q)}{\omega + E_\nu(k+q) - E_\mu(k) + i0^+}$$
$$\times \{f[E_\nu(k+q)] - f[E_\mu(k)]\}, \qquad (1)$$

where matrix elements $a_\mu^s(k) = \langle s|\mu k\rangle$ connect the orbital and the band spaces and are the components of the eigenvectors obtained from diagonalization of an effective tight-binding Hamiltonian derived from the DFT band structure via construction of maximally-localized Wannier functions. Here $f(E)$ is the Fermi distribution function, p, r, s, t are the orbital
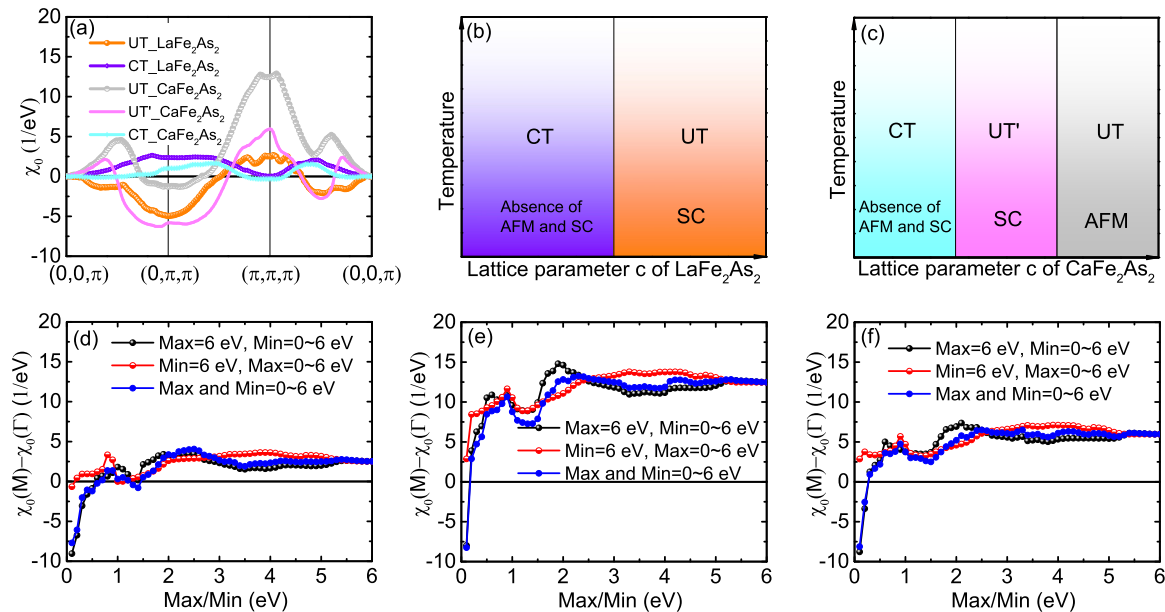
FIG. 2. Pauli susceptibilities with constant matrix element approximation $\chi_0(q, \omega = 0)$ (a). The schematic superconducting(SC), nonsuperconducting and nonmagnetic phase diagram of $LaFe_2As_2$ (b). The schematic superconducting(SC), antiferromagnetic(AFM), non-superconducting and nonmagnetic phase diagram of $CaFe_2As_2$ (c). The relative intensity of $\chi_0(q, \omega = 0)$ between (π, π, π) and $(0, 0, \pi)$ in different energy windows [-Min,Max] for the UT phase of $LaFe_2As_2$ (d), the UT phase of $CaFe_2As_2$ (e), and the UT′ phase of $CaFe_2As_2$ (f).

indices and μ, ν the band indices. q and k are the momentum vectors in the Brillouin zone, and N is the number of Fe lattice sites. It is found that off-diagonal elements of Pauli susceptibility are negligibly small compared to the diagonal ($p = s$, $r = t$) elements representing intraorbital and interorbital particle-hole excitations [31]. So in this paper, we focus on the intraorbital and interorbital particle-hole excitations and discuss their relations with magnetism and superconductivity. In fact, it is the relative intensity of Pauli susceptibility at some specific point in the Brillouin Zone determines the instability of the system, so in this paper we take the intensity of the Pauli susceptibility at $(0, 0, \pi)$ as the reference and discuss the relative intensity of Pauli susceptibility in different cases. We fix $q_z = \pi$ in the calculations and checked that the conclusions drawn below will not be changed if $q_z = 0$ is fixed.

The orbital occupation number is calculated by

$$n_{im} = c_{im}^{\dagger} c_{im}, \qquad (2)$$

where $c_{im}^{\dagger}(c_{im})$ creates(annihilates) an electron in orbital m of site i.

III. RESULTS AND DISCUSSIONS

The Pauli susceptibility signifying the particle-hole excitations is essential to understand the magnetism and superconductivity of iron-based superconductors [30–33]. Here we compare the Pauli susceptibility $\chi_0(q, \omega = 0)$ with constant matrix element approximation of both $LaFe_2As_2$ and $CaFe_2As_2$ in Fig. 2(a). The schematic phase diagrams of the two compounds are shown in Figs. 2(b) and 2(c). As is known, the Pauli susceptibilities within constant matrix elements approximation, where all the matrix elements in Eq. (1) are fixed to be one, can be used to quantify the nesting properties of the Fermi surfaces [34,35]. A peak present in

this Pauli susceptibility denotes that the Fermi surfaces are well nested by shifting a wave vector given by the position of the peak, and Pauli susceptibility brings more quantitative information than the Fermi surfaces. We can see the UT $CaFe_2As_2$ show a prominent peak at (π, π, π), supporting the stripe-type magnetic order at low temperature [20,21]. Although the peak at (π, π, π) is obviously suppressed in UT′ $CaFe_2As_2$ and UT $LaFe_2As_2$, there is still notable intensity around (π, π, π), which can provide the paring glue below Tc of superconductivity. Our results are consistent with the calculated noninteracting susceptibility of UT LaFe2As2 [15], and support the scenario that the uncollapsed tetragonal phase of $CaFe_2As_2$ stabilized by nonhydrostatic pressure is responsible for superconductivity as previous studies suggested [23,36]. For the nonsuperconducting and nonmagnetic CT $LaFe_2As_2$ and CT $CaFe_2As_2$, we can see no prominent peaks appear in $\chi_0(q, \omega = 0)$, implying no prominent instability in CT $LaFe_2As_2$ and CT $CaFe_2As_2$. Our results prove the view that spin fluctuations from itinerant electrons are essential to superconductivity for both $LaFe_2As_2$ and $CaFe_2As_2$.

To clarify which states around the Fermi level determine the properties of $\chi_0(q, \omega = 0)$ in these materials, we study the evolution of the relative intensity at (π, π, π) of χ_0 with different energy windows around the Fermi level for UT phase of $LaFe_2As_2$ and both UT and UT′ phases of $CaFe_2As_2$ as shown in Figs. 2(d)–2(f). Interestingly, the particle-hole excitations are unexpectedly found to condense at $(0, 0, \pi)$ rather than (π, π, π) if only the states in a small energy window are calculated. We can see as the energy window become larger, the relative intensity at (π, π, π) changes from negative to positive and become converged at about 5 eV. So only if the states in large enough energy windows are involved, then the particle-hole excitation condenses at (π, π, π), strongly suggesting considering only the states next to the Fermi level
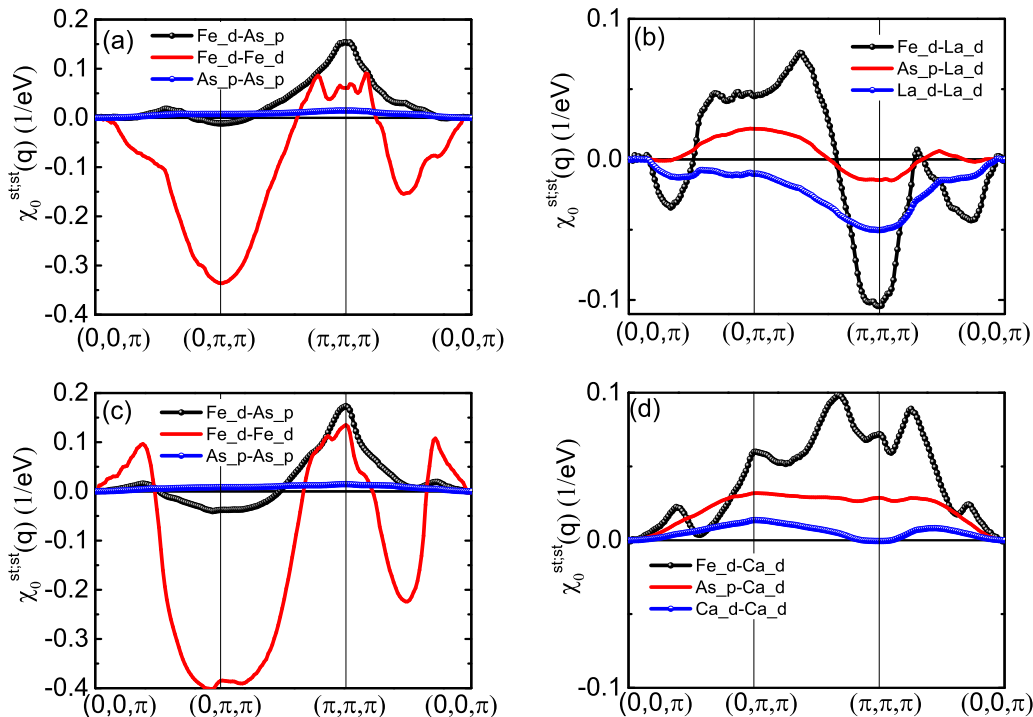
FIG. 3. Atom resolved Pauli susceptibilities for the UT phase of LaFe$_2$As$_2$ (a), (b) and for the UT$'$ phase of CaFe$_2$As$_2$ (c), (d).

is not enough to capture the accurate instability of iron-based superconductors. We can see from the band structures as shown in Figs. 1(a)–1(d) and the density of states as shown Figs. 1(i)–1(l) that the 3d orbital from Fe, the 4p orbital from As, and the 3d orbital from Ca or 5d orbital from La entangle with each other, so the 4p orbital of As and 5d orbital of La or 3d orbital in Ca may also play important roles in the particle-hole excitations of these materials as well as the 3d orbital from Fe.

We also fix the energy above the Fermi level at 6.0 eV, and study the evolution of $\chi_0(q, \omega = 0)$ with different energies below the Fermi level. And we then fix the energy below the Fermi level at 6.0 eV, and study the evolution of $\chi_0(q, \omega = 0)$ with different energies above the Fermi level. We can see in Figs. 2(d)–2(f) the condensations of the particle-hole excitations are also not converged if only the states in a small energy window above or below the Fermi level is calculated. So both the states around the Fermi level in a wide energy range are important to the condensation properties of the particle-hole excitation.

To clarify how the p orbital of As and the interlayer cation Ca or La affect the superconducting properties, we study the interorbital particle-hole excitations $\chi_0^{st;st}(q, \omega = 0)$ between different atoms for the UT phase of LaFe$_2$As$_2$ and UT$'$ phase of CaFe$_2$As$_2$ as shown in Fig. 3. Surprisingly and interestingly, the total relative intensity at (π, π, π) of the interorbital particle-hole excitations $\chi_0^{st;st}(q, \omega = 0)$ between the 3d orbital of Fe and 4p orbital of As is much larger than the intraorbital and interorbital particle-hole excitations $\chi_0^{st;st}(q, \omega = 0)$ within the 3d orbital of Fe for both UT LaFe$_2$As$_2$ and UT$'$ CaFe$_2$As$_2$ as shown in Figs. 3(a) and 3(c). Therefore, the interorbital particle-hole excitations between the 3d orbital of Fe and 4p orbital of As may play a key role

in providing fluctuations for electron-pairing. This is the first time that such a fundamental relation between the 4p states of As and $\chi_0^{st;st}(q, \omega = 0)$ for the large relative instability at (π, π, π) is derived.

On the other hand, the 5d states of La in the UT phase of LaFe$_2$As$_2$ and the 3d states of Ca in the UT$'$ phase of CaFe$_2$As$_2$ also surprisingly play an essential role in the relative intensity at (π, π, π) of $\chi_0^{st;st}(q, \omega = 0)$. We can see all the relative intensities at (π, π, π) of $\chi_0^{st;st}(q, \omega = 0)$ involved with the 5d orbital of La are negative in the UT phase of LaFe$_2$As$_2$ as shown in Fig. 3(b), whereas the interorbital particle-hole excitations between the 3d orbital of Ca and 3d orbital of Fe or 4p orbital of As condense positively around (π, π, π) in the UT$'$ phase of CaFe$_2$As$_2$ as shown in Fig. 3(d). Thus the intercalating cations Ca and La contribute contrarily to the relative intensities at (π, π, π) of $\chi_0^{st;st}$.

The role of the 3d orbital of Fe, 4p orbital of As and 3d orbital of Ca of 5d orbital of La is further studied by calculating susceptibility $\chi_0^{st;st}(q, \omega = 0)$ in different energy windows around the Fermi level. We plot the evolution of the relative intensity at (π, π, π) of $\chi_0^{st;st}(q, \omega = 0)$ with different energy windows for the UT phase of LaFe$_2$As$_2$ and the UT$'$ phase of CaFe$_2$As$_2$ in Fig. 4, where s and t denote the 3d orbital of Fe, the 4p orbital of As, and the 3d orbital of Ca or the 5d orbital of La respectively. For both the UT phase of LaFe$_2$As$_2$ and the UT$'$ phase of CaFe$_2$As$_2$, the particle-hole excitations from 3d electrons of Fe show strong ferromagnetic instability when the energy window is small, and converge to condense around (π, π, π) only when the energy window is above 3.5 eV. For both the UT phase of LaFe$_2$As$_2$ and the UT$'$ phase of CaFe$_2$As$_2$, the relative intensity at (π, π, π) of the interorbital susceptibility $\chi_0^{st;st}(q, \omega = 0)$ between the 3d orbital of Fe and the 4p orbital of As converge at (π, π, π)
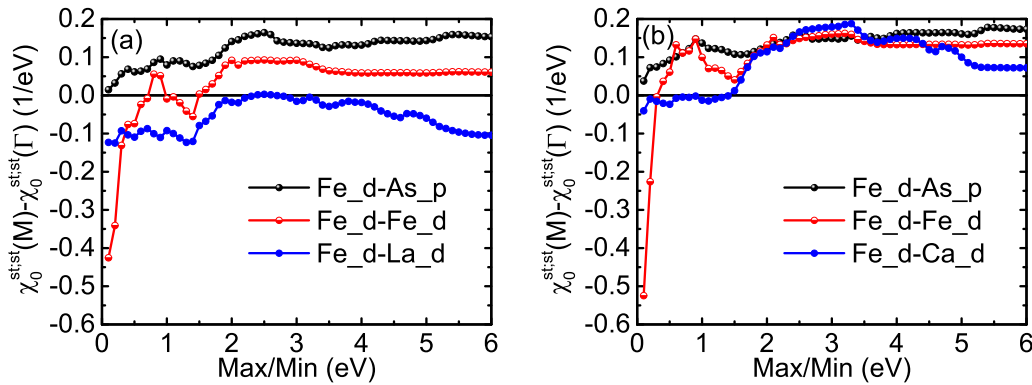
FIG. 4. The relative intensity of atom resolved Pauli susceptibilities in different energy windows $[-\text{Min}, \text{Max}]$ for the UT phase of $LaFe_2As_2$ (a) and the UT′ phase of $CaFe_2As_2$ (b).

when the energy window is above 5 eV. For the UT phase of $LaFe_2As_2$, the relative intensity at (π, π, π) of interorbital susceptibility $\chi_0^{st;st}(q, \omega = 0)$ between the 3d orbital of Fe and the 5d orbital of La is negative when the energy window is small, and becomes positive when the energy window is larger than 1.9eV, but finally converge to be negative. For the UT′ phase of $CaFe_2As_2$, the relative intensity at (π, π, π) of interorbital susceptibility $\chi_0^{st;st}(q, \omega = 0)$ between the 3d orbital of Fe and the 3d orbital of Ca show maxima at 3.3 eV and finally converge to be positive. These results indicate that all the electrons in the 3d orbital of Fe, 4p orbital of As, and 3d orbital of Ca or 5d orbital of La in a large enough energy range contribute to the relative intensity at (π, π, π) of $\chi_0^{st;st}(q, \omega = 0)$. We have further shown in the Appendix B

that some weight that actually sits on the As 4p orbitals was transferred to Fe 3d orbitals in models without As 4p orbitals, leading to losing the fact that As 4p orbitals actually contribute to the instability at (π, π, π) substantially. Thus to accurately characterize the instabilities of the compounds we studied, a large energy window including the As 4p orbitals should be adopted.

Since both the intraorbital and interorbital particle-hole excitations can provide the glue for electron-pairing of superconductivity [30], we further study the interorbital particle-hole excitations of $\chi_0^{st;st}(q, \omega = 0)$ to extract which partial orbitals play dominant role in the instability at (π, π, π). The primary interorbital Pauli susceptibilities are plotted in Fig. 5. We can see for UT $LaFe_2As_2$, the in-
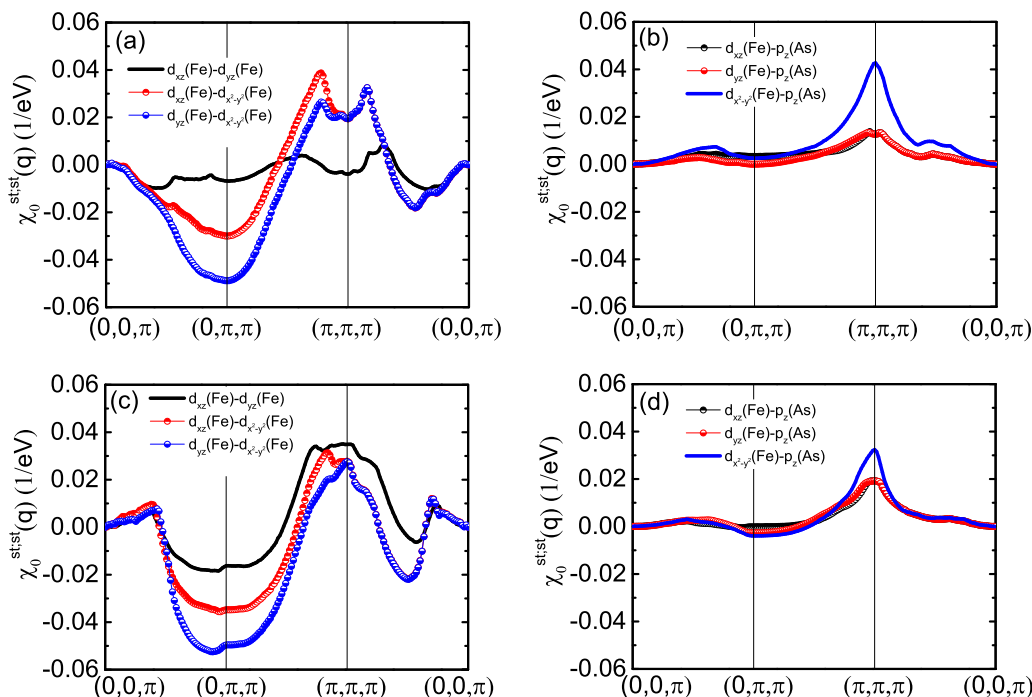
FIG. 5. The primary interorbital Pauli susceptibilities from the 3d orbital of Fe for the UT phase of $LaFe_2As_2$ (a) and the UT′ phase of $CaFe_2As_2$(c). The primary interorbital Pauli susceptibilities between the 3d orbital of Fe and the 4p orbital of As for the UT phase of $LaFe_2As_2$ (b) and the UT′ phase of $CaFe_2As_2$(d).
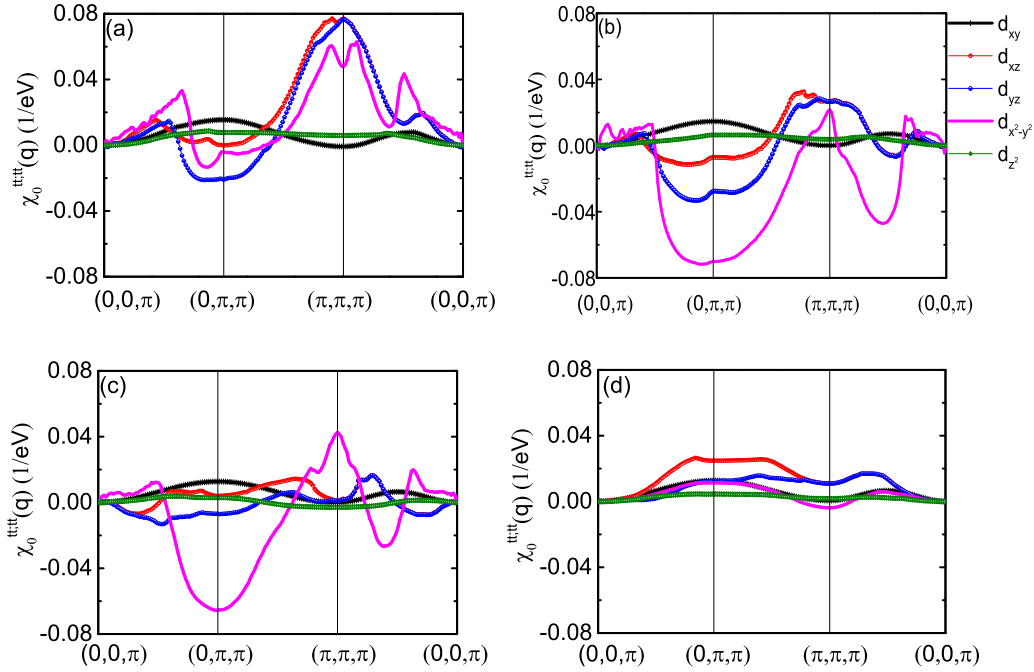
FIG. 6. Intraorbital Pauli susceptibilities of the 3d orbital of Fe for the UT phase of $CaFe_2As_2$ (a), the UT$'$ phase of $CaFe_2As_2$ (b), the UT phase of $LaFe_2As_2$ (c), and the CT phase of $LaFe_2As_2$ (d).

terorbital particle-hole excitations between $d_{x^2-y^2}$ orbital and d_{xz} or d_{yz} orbital condense around (π, π, π), while the condensation of interorbital particle-hole excitations between d_{xz} and d_{yz} orbitals around (π, π, π) is much weaker as shown in Fig. 5(a). The interorbital particle-hole excitations between any two orbitals from $d_{x^2-y^2}$ orbital, d_{xz} or d_{yz} orbital all strongly condense at (π, π, π) for UT$'$ $CaFe_2As_2$ as shown in Fig. 5(c). It is noteworthy to mention that the interorbital particle-hole excitations between the $4p_z$ orbital of As and the 3d orbitals $d_{x^2-y^2}$, d_{xz} or d_{yz} of Fe also show comparable intensity of condensation at (π, π, π) for both UT $LaFe_2As_2$ and UT$'$ $CaFe_2As_2$ as shown in Figs. 5(b) and 5(d), which strongly suggests that the $4p_z$ states of As may be relevant to superconductivity in these two iron-based superconductors.

Because magnetism is related to the intraorbital particle-hole excitations $\chi_0^{pr;st}(q, \omega = 0)$ with $p = r = s = t$ [31], we now focus on $\chi_0^{tt;tt}$ to discuss the microscopic origin of magnetism in these materials. We can see a well-defined instability at (π, π, π) in the d_{xz} and d_{yz} orbitals in UT phase of $CaFe_2As_2$ as shown in Fig. 6(a), leading to the tendency to form stripe-type anti-ferromagnetic order at low temperature. When it comes to the UT$'$ phase of $CaFe_2As_2$ as shown in Fig. 6(b), $\chi_0^{tt;tt}$ of d_{xz} and d_{yz} orbital shows a widely broadened maxima around (π, π, π), while only a small instability at (π, π, π) in the $d_{x^2-y^2}$ orbital. For the UT phase of $LaFe_2As_2$ only $\chi_0^{tt;tt}$ of the $d_{x^2-y^2}$ orbital show a peak at (π, π, π) as shown in Fig. 6(c). So the instability at (π, π, π) from intraorbital particle-hole excitations in the UT phase of $LaFe_2As_2$ and UT$'$ phase of $CaFe_2As_2$ is not strong enough to induce the stripe-type anti-ferromagnetic order but may still provide spin fluctuations helping the electron-pairing together with instabilities around (π, π, π) from interorbital particle-hole excitations. No prominent peak can be observed in the

intraorbital particle-hole excitations of the CT phase of $LaFe_2As_2$ as shown in Fig. 6(d).

Finally we want to discuss the doping effect in these iron-based materials. It is found that hole doping did not decrease electron occupations of all the five 3d orbitals of Fe [37]. Here we study the electron doping effect by constructing tight-binding models consisting of La 5d orbital, Fe 3d orbital, and As 3p orbital from first-principles calculations as displayed in Fig. 7. We can see from Fig. 7(a) that electrons in the d_{xz}/d_{yz}, $d_{x^2-y^2}$ and d_{z^2} orbitals increase in the CT phase compared with the UT phase for $LaFe_2As_2$, and this trend also applies to the UT$'$ phase compared with the UT phase for $CaFe_2As_2$. Meanwhile, there are more electrons in the d_{xz}/d_{yz} and d_{z^2} orbitals but fewer electrons in the d_{xy} and d_{z^2} orbitals of Fe in $LaFe_2As_2$ compared with $CaFe_2As_2$. There are substantial electrons in the 5d orbital of La and 3d orbital of Ca as shown in Figs. 7(b) and 7(c). From Figs. 7(d) and 7(e) we can see that the total electrons in the 3d orbital of Fe in $LaFe_2As_2$ are more than that in $CaFe_2As_2$, but the total electrons in the 4p orbital of As in $LaFe_2As_2$ are less than that in $CaFe_2As_2$ for the UT and UT$'$ phases respectively. The total electron occupations in the 3d orbital of Fe and 4p orbital of As in $CaFe_2As_2$ change little compared with that in $LaFe_2As_2$ as shown in Fig. 7(f). So the one 5d orbital electron of La does not effectively dope to the Fe-As layers. The main difference among the various phases of $LaFe_2As_2$ and $CaFe_2As_2$ is the re-distribution of electrons among the partial orbitals, leading to their different band structures in a wide energy range.

IV. CONCLUSIONS

In this work, we carry out a comparative DFT study on the different phases of $LaFe_2As_2$ and the counterpart $CaFe_2As_2$. The orbital and atom resolved Pauli susceptibilities and their
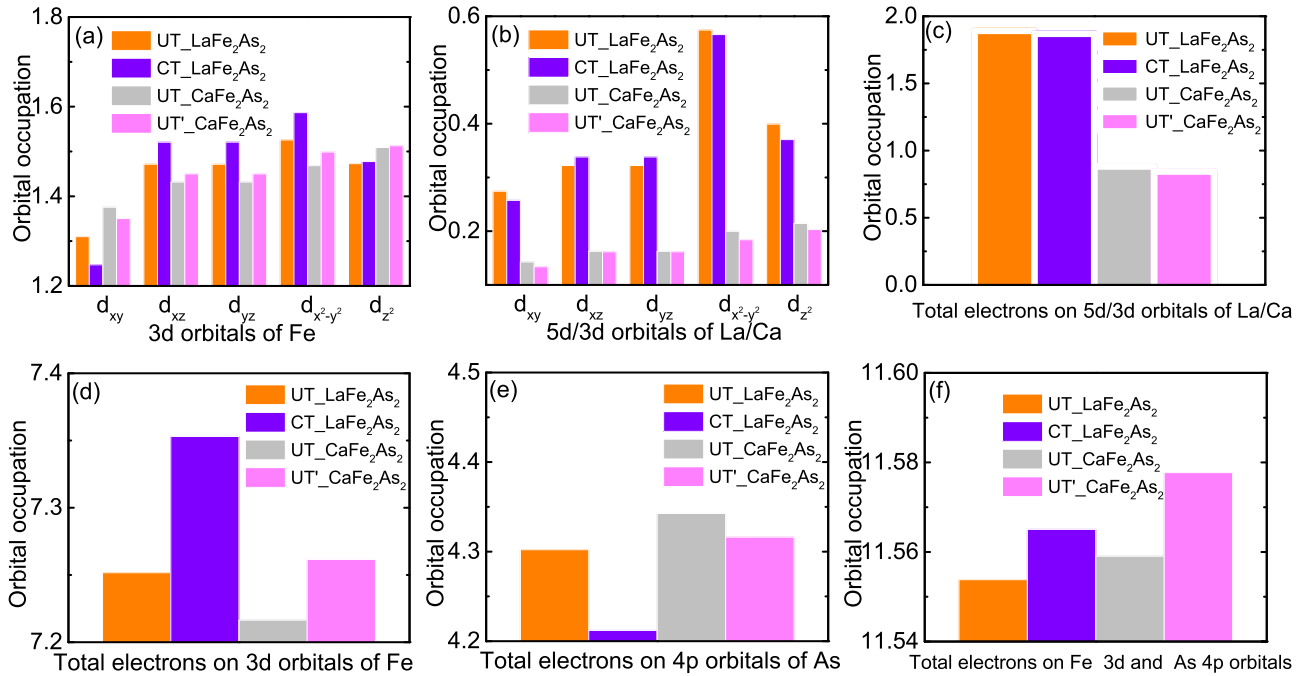
FIG. 7. Charge occupations of the five 3d orbitals of Fe (a). Charge occupations of the five 3d orbitals of Ca or 5d orbitals of La (b). The total charge occupations of the 3d orbitals of Ca or 5d orbitals of La (c). The total charge occupations of the 3d orbitals of Fe (d). The total charge occupations of the 4p orbitals of As (e). The total charge occupations of the 3d orbitals of Fe and the 4p orbitals of As (f).

relationship with magnetism and superconductivity have been investigated. The main results of our study are as follows.

(1) We find that the interorbital particle-hole excitations between the 4p orbital of As and the 3d orbital of Fe play an important role in the prominent instability at (π, π, π), strongly suggesting the 4p states of As are relevant to superconductivity in iron-based superconductors.

(2) We also find the 3d states of Ca and 5d states of La play contrary contributions to the instability at (π, π, π) which act as the pairing glue for superconductivity. The 3d states of Ca enhance the instability at (π, π, π) while the 5d states of La weaken the instability at (π, π, π).

(3) We find the 5d orbital electron of La remains in the 5d orbital and does not dope to the 3d orbital of Fe, but electrons re-distribute among the partial orbitals in different phases of $LaFe_2As_2$ and $CaFe_2As_2$, which may be the origin of different magnetic and superconducting properties of these iron-based materials.

Our results show that the relative condensation intensity around (π, π, π) of the particle-hole excitations is a key parameter in determining superconductivity or magnetism for $LaFe_2As_2$ and $CaFe_2As_2$. To our knowledge, the relationship between the relative instability around (π, π, π) of $\chi_0^{st;st}(q, \omega = 0)$ and the 4p states of As or the interlayer cations states was first found in our work and has never been revealed before. This means that considering only the 3d states of Fe is not enough to fully understand superconductivity in iron-based superconductors. Our results are interesting in two aspects. First, the signatures of the large relative instability of $\chi_0^{st;st}(q, \omega = 0)$ related to the 4p states of As or the interlayer cations states pose a challenge to the models with only 3d orbital of Fe and prove the need to establish more accurate models. Second, our results also suggest that iron-based

superconductors with strong instability around (π, π, π) from interorbital particle-hole excitations but small instability at a specific point in the Brillouin Zone from intraorbital particle-hole excitations would show high Tc of superconductivity.

V. THE INPUT FOR WANNIER90 TO CALCULATE THE EFFECTIVE TIGHT-BINDING MODEL

A 1331 k mesh is used for WANNIER90, and we find the results show convergence with the k mesh we used in the paper by testing larger k meshes. The upper bound of the frozen energy window for the disentanglement is set to be 3.6 eV to preserve exactly the properties of all the compounds we studied. All other inputs for WANNIER90 are set to be the default ones.

VI. RESULTS OF THE EFFECTIVE TIGHT-BINDING MODELS WITHOUT THE P ORBITALS OF AS

The results of a tight-binding model without the As 4p orbitals for the UT phase of $LaFe_2As_2$ as shown in Fig. 8. A 1331 k mesh is used for WANNIER90, and larger k meshes have been tested for convergence. The frozen energy window for the disentanglement is $(-0.9 \text{ eV}, 0.9 \text{ eV})$ for the Fe 3d orbitals tight-binding model, and $(-1.4 \text{ eV}, 3.6 \text{ eV})$ for the tight-binding model including Fe 3d orbitals and La 5d orbitals. Both the band structures and density of states obtained from first principles calculation and effective tight-binding model with only Fe 3d orbitals show general but not perfect consistency with each other as presented in Figs. 8(a) and 8(c), indicating the discrepancy of the effective tight-binding model with only Fe 3d orbitals and the necessity to consider weights
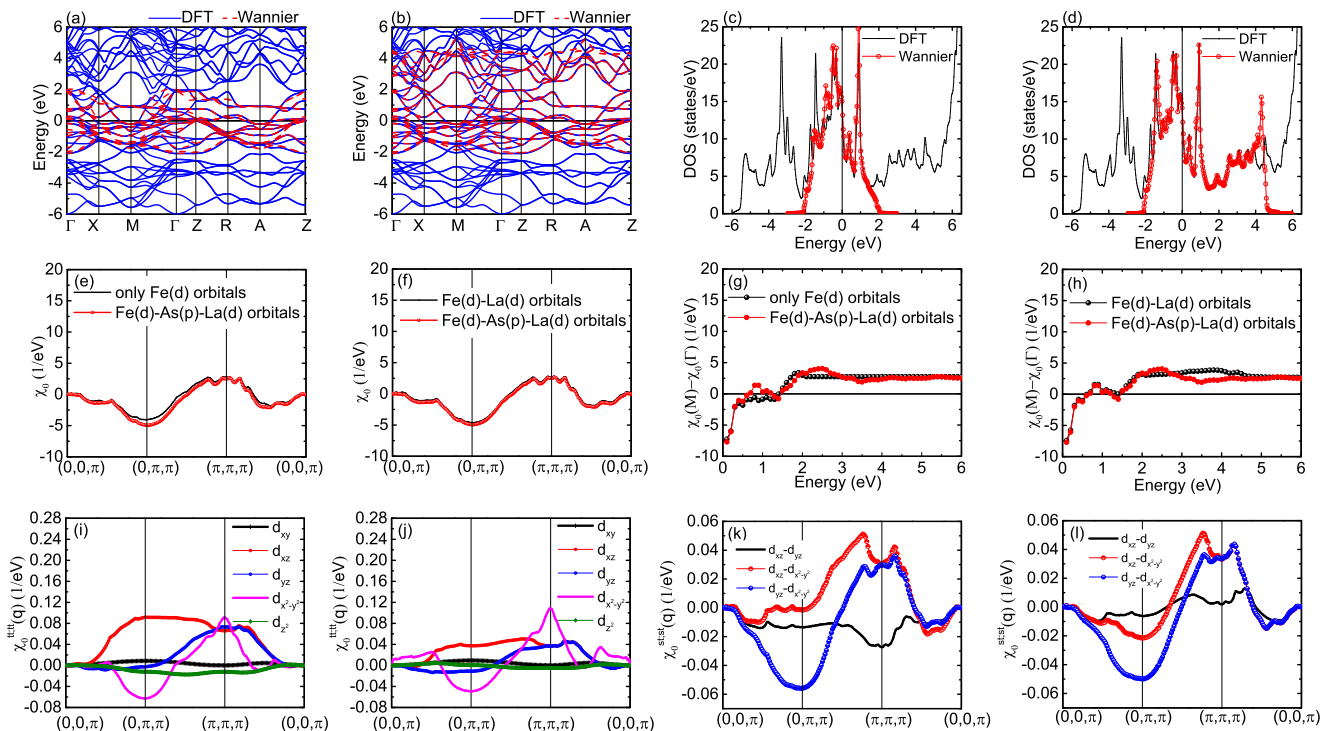
FIG. 8. Comparison of band structure calculated from density functional theory and effective Fe 3d orbitals tight-binding model (a) and effective Fe 3d orbitals and La 5d orbitals tight-binding model (b) for the UT phase of LaFe$_2$As$_2$. Comparison of density of states calculated from density functional theory and effective Fe 3d orbitals tight-binding model (c) and effective Fe 3d orbitals and La 5d orbitals tight-binding model (d) for the UT phase of LaFe$_2$As$_2$. Comparison of Pauli susceptibilities with constant matrix element approximation derived from different effective tight-binding models for the UT phase of LaFe$_2$As$_2$ (e), (f). Comparison of the relative intensity of $\chi_0(q, \omega = 0)$ between (π, π, π) and $(0, 0, \pi)$ in different energy windows $[-$Min, Max$]$ derived from different effective tight-binding models for the UT phase of LaFe$_2$As$_2$ (g, h) with Max/Min $= (0, 6$ eV$)$. Intraorbital Pauli susceptibilities of the 3d orbital of Fe for the UT phase of LaFe$_2$As$_2$ derived from effective Fe 3d orbitals tight-binding model (i), and from effective Fe 3d orbitals and La 5d orbitals tight-binding model (j). The primary interorbital Pauli susceptibilities from the 3d orbital of Fe for the UT phase of LaFe$_2$As$_2$ derived from effective Fe 3d orbitals tight-binding model (k), and from effective Fe 3d orbitals and La 5d orbitals tight-binding model (l).

of each eigenstate contributed from As 4p orbitals and and La 5d orbitals.

The susceptibility with constant matrix element approximation coincide with each other in different tight-binding models as shown in Figs. 8(e) and 8(f) and converge in smaller energy windows derived from the models without the As 4p orbitals as shown in Figs. 8(g) and 8(h). However, the intraorbital and interorbital susceptibilities of Fe 3d orbitals in Figs. 8(i)–8(l) show apparent discrepancies compared with the results from tight-binding model including Fe 3d orbitals, La 5d orbitals and As 4p orbitals as shown in Figs. 5(a) and 6(c). As shown in Figs. 8(i) and 8(j), the instability of $\chi_0^{tt;tt}$ at (π, π, π) from $d_{x^2-y^2}$, d_{xz} and d_{yz} orbitals is higher than that in Fig. 6(c). There is also a broadened maxima around $(0, \pi, \pi)$ of $\chi_0^{tt;tt}$ from d_{yz} orbital as shown in Fig. 8(i). The reason for these discrepancies is that contributions to susceptibilities from the As 4p orbitals and La 5d orbitals are transferred to the Fe 3d orbitals in the only Fe 3d orbitals model, which also results in the higher instability around (π, π, π) of the

interorbital susceptibilities between $d_{x^2-y^2}$ orbital and d_{xz} or d_{xz} orbital, and the negative minimum around (π, π, π) of the interorbital susceptibility between d_{xz} and d_{xz} orbitals as shown in Fig. 8(k).

Now we consider a tight-binding model including Fe 3d orbitals and La 5d orbitals, and we can see the contributions to susceptibilities from the As 4p orbitals are transferred to the Fe 3d orbitals as manifested by the larger instabilities around (π, π, π) of both intraorbital and interorbital susceptibilities from $d_{x^2-y^2}$, d_{xz} and d_{xz} orbitals as shown in Figs. 8(j) and 8(l) than those shown in Figs. 5(a) and 6(c).

[1] R. M. Fernandes, A. I. Coldea, H. Ding, I. R. Fisher, P. J. Hirschfeld, and G. Kotliar, Nature (London) **601**, 35 (2022).

[2] M. Yi, Y. Zhang, Z. X. Shen, and D. H. Lu, npj Quant. Mater. **2**, 57 (2017).

[3] T. Shimojima, F. Sakaguchi, K. Ishizaka, Y. Ishida, T. Kiss, M. Okawa, T. Togashi, C. T. Chen, S. Watanabe, M. Arita, K. Shimada, H. Namatame, M. Taniguchi, K. Ohgushi, S. Kasahara, T. Terashima, T. Shibauchi, Y. Matsuda, A. Chainani, and S. Shin, Science **332**, 564 (2011).

[4] D. J. Singh and M. H. Du, Phys. Rev. Lett. **100**, 237003 (2008).

[5] H. Eschrig and K. Koepernik, Phys. Rev. B **80**, 104503 (2009).

[6] M. Daghofer, A. Moreo, J. A. Riera, E. Arrigoni, D. J. Scalapino, and E. Dagotto, Phys. Rev. Lett. **101**, 237004 (2008).

[7] O. Vafek and A. V. Chubukov, Phys. Rev. Lett. **118**, 087003 (2017).

[8] M. Daghofer, A. Nicholson, A. Moreo, and E. Dagotto, Phys. Rev. B **81**, 014511 (2010).

[9] M. M. Korshunov, Y. N. Togushova, and I. Eremin, J. Supercond. Nov. Magn. **26**, 2665 (2013).

[10] E. Bascones, B. Valenzuela, and M. J. Calderón, Phys. Rev. B **86**, 174508 (2012).

[11] Q. L. Luo, K. Foyevtsova, G. D. Samolyuk, F. Reboredo, and E. Dagotto, Phys. Rev. B **90**, 035128 (2014).

[12] C. Cao, P. J. Hirschfeld, and H. P. Cheng, Phys. Rev. B **77**, 220506 (2008).

[13] D. Guterding, H. O. Jeschke, I. I. Mazin, J. K. Glasbrenner, E. Bascones, and R. Valentí, Phys. Rev. Lett. **118**, 017204 (2017).

[14] A. Iyo, S. Ishida, H. Fujihisa, Y. Gotoh, I. Hase, Y. Yoshida, H. Eisaki, and K. Kawashima, J. Phys. Chem. Lett. **10**, 1018 (2019).

[15] I. I. Mazin, M. Shimizu, N. Takemori, and H. O. Jeschke, Phys. Rev. Lett. **123**, 267001 (2019).

[16] J. Z. Zhao, Y. L. Wang, X. L. Feng, and S. Y. A. Yang, Phys. Rev. B **103**, 125125 (2021).

[17] S. Acharya, D. Pashov, F. Jamet, and M. van Schilfgaarde, Phys. Rev. Lett. **124**, 237001 (2020).

[18] H. Usui and K. Kuroki, Phys. Rev. Res. **1**, 033025 (2019).

[19] I. Pallecchi, A. Iyo, H. Ogino, M. Affronte, M. Putti, Phys. Rev. Mater. **4**, 114803 (2020).

[20] A. Kreyssig, M. A. Green, Y. Lee, G. D. Samolyuk, P. Zajdel, J. W. Lynn, S. L. Bud'ko, M. S. Torikachvili, N. Ni, S. Nandi, J. B. Leão, S. J. Poulton, D. N. Argyriou, B. N. Harmon, R. J. McQueeney, P. C. Canfield, and A. I. Goldman, Phys. Rev. B **78**, 184517 (2008).

[21] D. K. Pratt, Y. Zhao, S. A. J. Kimber, A. Hiess, D. N. Argyriou, C. Broholm, A. Kreyssig, S. Nandi, S. L. Bud'ko, N. Ni, P. C. Canfield, R. J. McQueeney, and A. I. Goldman, Phys. Rev. B **79**, 060510 (2009).

[22] M. S. Torikachvili, S. L. Bud'ko, Ni Ni, and Paul C. Canfield, Phys. Rev. Lett. **101**, 057006 (2008).

[23] K. Prokeš, A. Kreyssig, B. Ouladdiaf, D. K. Pratt, N. Ni, S. L. Bud'ko, P. C. Canfield, R. J. McQueeney, D. N. Argyriou, and A. I. Goldman, Phys. Rev. B **81**, 180506 (2010).

[24] J. H. Soh, G. S. Tucker, D. K. Pratt, D. L. Abernathy, M. B. Stone, S. Ran, S. L. Bud'ko, P. C. Canfield, A. Kreyssig, R. J. McQueeney, and A. I. Goldman, Phys. Rev. Lett. **111**, 227002 (2013).

[25] K. Schwarz, P. Blaha, and G. K. H. Madsen, Comput. Phys. Commun. **147**, 71 (2002).

[26] J. P. Perdew, K. Burke, and M. Ernzerhof, Phys. Rev. Lett. **77**, 3865 (1996).

[27] A. A. Mostofi, J. R. Yates, Y. S. Lee, I. Souza, D. Vanderbilt, and N. Marzari, Comput. Phys. Commun. **178**, 685 (2008).

[28] J. Kuneš, R. Arita, P. Wissgott, A. Toschi, H. Ikeda, and K. Held, Comput. Phys. Commun. **181**, 1888 (2010).

[29] S. R. Saha, N. P. Butch, T. Drye, J. Magill, S. Ziemak, K. Kirshenbaum, P. Y. Zavalij, J. W. Lynn, and J. Paglione, Phys. Rev. B **85**, 024525 (2012).

[30] S. Graser, T. A. Maier, P. J. Hirschfeld, and D. J. Scalapino, New J. Phys. **11**, 025016 (2009).

[31] M. C. Ding, H. Q. Lin, and Y. Z. Zhang, Phys. Rev. B **87**, 125129 (2013).

[32] I. I. Mazin, D. J. Singh, M. D. Johannes, and M. H. Du, Phys. Rev. Lett. **101**, 057003 (2008).

[33] M. C. Ding and Y. Z. Zhang, Phys. Rev. B **89**, 085120 (2014).

[34] Y. Z. Zhang, I. Opahle, H. O. Jeschke, and R. Valentí, Phys. Rev. B **81**, 094505 (2010).

[35] Y. Z. Zhang, H. P. Lee, I. Opahle, H. O. Jeschke, and R. Valentí, J. Phys. Chem. Solids **72**, 324 (2011).

[36] A. Sanna, G. Profeta, S. Massidda, and E. K. U. Gross, Phys. Rev. B **86**, 014507 (2012).

[37] M. C. Ding, L. M. Wu, G. Zhao, B. Y. Pan, and Y. Z. Zhang, Europhys. Lett. **133**, 17004 (2021).